Effect of geometric curvature on vitrification behavior for polymer nanotubes confined in anodic aluminum oxide templates

Jiao Chen, Linling Li, Dongshan Zhou, Xiaoliang Wang,* and Gi Xue*

Department of Polymer Science and Engineering, School of Chemistry and Chemical Engineering, Key Laboratory of High Performance Polymer Materials and Technology (Nanjing University), Ministry of Education, Nanjing National Laboratory of Microstructures, Nanjing University, Nanjing 210093, People's Republic of China

(Received 8 May 2015; published 14 September 2015)

The glass transition behavior of polystyrene (PS) nanotubes confined in cylindrical alumina nanopores was studied as a function of pore diameter (d) and polymer tube thickness (δ). Both the calorimetric glass transition temperature and the microstructure measured by a nonradiative energy transfer method indicated that the polymer nanotube, or concave polymer thin film, exhibited significant differences in vitrification behavior compared to the planar one. A closer interchain proximity and an increased T_g were observed for polymer nanotubes with respect to the bulk polymer. T_g for polymer nanotubes was primarily dependent on the curvature radius d of the template, while it was less dependent on the thickness δ of the PS tube wall in the range of 11–23 nm. For small nanotubes ($d = 55$ nm), the T_g increased as high as 18 °C above the bulk value. This vitrified property reverted back to the bulk value when the substrate was chemically removed, which indicated the crucial importance of the interfacial effect imposed by the hard wall with a concave geometry.

DOI: 10.1103/PhysRevE.92.032306 PACS number(s): 64.70.pj, 65.80.−g, 68.35.bm

I. INTRODUCTION

Confined at the nanoscale, polymer films show peculiar behaviors characterized by shifts in the glass transition temperature (T_g) and dramatic changes in other physical properties with respect to bulk polymers [1–10]. Despite significant studies in this area, many issues, particularly the intrinsic conformation of polymer influenced by pure size effect and how it changes when they intersect the interface, remain unclear.

Due to the ease of processing, most studies have focused on the T_g of planar thin films and corresponding nanoparticles [11,12], while relatively few studies have focused on extending investigations beyond planar thin films to other geometric shapes, such as concave films in nanotubes or nanobowls [13–16]. As other geometric shapes are used more frequently in technologies ranging from molecular transport to ultrafiltration to plastic electronics, a greater understanding of the influences of geometrical difference on dynamics is necessary and significant. Nanoporous anodic aluminum oxide (AAO) templates, which can be infiltrated with polymers to produce nanotubes or nanofibers, offer a uniquely well-defined environment for the investigation of a concave geometry confinement. The confinement effects on the polymer chain conformation can affect the interfacial properties and ultimately, the long-term stability of the nanostructured materials [17]. This confinement influences numerous properties and processes in materials science, including rubber elasticity, ultrafiltration, and even in biology (e.g., the folding of protein chains and the packing of genomes into viral capsids) [18]. Chen and Russell presented a simple, cost-effective method to fabricate poly(3-hexylthiophene) (P3HT) nanostructures by using AAO templates [19]. They removed the templates to obtain freestanding P3HT nanorod arrays used to fabricate organic photovoltaic (OPV) devices.

Simulations have revealed that the conformation of polymer chains is expected to be perturbed near a hard wall [18,20,21]. Several techniques have been used for probing the chain configuration of polymer thin films [22,23]. However, these techniques are appropriate for structural analysis only in the vicinity of a surface or an interface. Boucher *et al.* [24] found a T_g depression for polystyrene (PS) thin films by differential scanning calorimeter (DSC), while there was no depression with broadband dielectric spectroscopy (BDS). The recent review by Kremer *et al.* [25] also mentioned that changes in the T_g measured by DSC (or related techniques) are usually observed in nanostructured systems, whereas the so-called dynamic T_g measured by techniques, such as dielectric spectroscopy, does not change. So for thin films under confinement, there is a T_g depression but invariant segmental dynamics. It remains quite a challenge to unambiguously and directly determine the chain conformations of polymer thin films. Neutron scattering is a relatively ideal technique to directly access the polymer conformation. It can powerfully and unambiguously provide information on the overall polymer conformation. Moreover, the surface signal can also be identified. Shin *et al.* found that the large chain molecules confined in AAO had an enhanced mobility by the small-angle neutron scattering (SANS) technique [17]. Martin *et al.* directly observed the single-chain dynamics of entangled polymer chains confined in cylindrical nanopores with neutron spin echo [26]. In a recent perspective, Ediger and Forrest pointed out that new and highly creative methods are required to directly measure important material properties in thin films [27]. To address the current challenge in probing chain conformations at the nanoscale, here we report a fluorescence nonradiative energy transfer (NRET) method to amplify the sensitivity of interchain proximity. This method was originally developed to study chain interpenetration in polymer films by Itagaki *et al.* [28–30]. It is an effective method for direct characterization of chain conformation for thin films, which is further correlated to the polymer dynamics under confinement.

*Authors to whom correspondence should be addressed. Email address: wangxiaoliang@nju.edu.cn, xuegi@nju.edu.cn

In our recent work [31], the glass transition behaviors of poly(methyl methacrylate) nanorods confined in alumina nanotube templates were systematically studied. After slow cooling the melt, two distinct T_gs occurred and they were lower and higher than the bulk value, respectively. However, fast cooling the melt resulted in only one single glass transition temperature. This was an unusual phenomenon to observe in nanopores. A two-layer model was further proposed to explain the phenomenon and it was found that polymers confined in nanoporous templates could have special glass transition behaviors. The pore size was much larger than the gyration radius (R_g) of polymer; however, the confinement effect on T_g was still observed. Similarly, Hofmann *et al.* [32] used the nuclear magnetic resonance (NMR) technique to detect the dynamics of polybutadiene in AAO and found a confinement effect although the size of the confinement was larger than the polymer size in the melt. Floudas *et al.* [33] investigated the dynamics of unentangled polymers confined in AAO with dielectric spectroscopy, and the distribution of relaxation times was also broadened by chain adsorption even within pores with size 50 times the chain dimension. So for such systems, though the size confinement effect can be negligible, the interfacial or adsorption effect still exists and results in a confinement effect on the glass transition as well.

In this work, our major focus is on the glass transition behavior of polystyrene nanotubes instead of nanorods in AAO templates. We investigate the effects of tube diameter and polymer tube thickness on glass transition dynamics (T_g) by using differential scanning calorimeter (DSC) analysis. Moreover, the NRET method is used to probe the interchain proximity, which well supports the T_g results.

II. EXPERIMENTAL SECTION

A. Materials

Monodisperse polystyrene (PS_{6k} : $M_n = 6\,kg/mol$, $d = 1.06$; PS_{60k} : $M_n = 61\,kg/mol$, $d = 1.05$) was purchased from Polymer Source Inc., Canada. These PS samples were labeled with a carbazolyl probe (PS_{6k}-Cz) or an anthryl probe (PS_{6k}-An). The mole fractions of the labels are 0.26% (PS_{6k}-Cz) and 0.11% (PS_{6k}-An), respectively. The details of the preparation can be found elsewhere [34]. Toluene was commercially purchased and distilled before use. Self-ordered AAO templates with different pore diameters (250, 130, and 55 nm) were purchased from Puyuan Nano Co. (Hefei, China). The membranes were rinsed with chloroform and methanol to remove possible impurities on the surfaces and then annealed at 150 °C for 2 h in vacuum before use.

B. Preparation of PS thin films and nanotubes

Films with different thicknesses were prepared by spin coating PS from purified toluene solution. Their thicknesses were altered by changing the original solution concentrations and measured with ellipsometry (JASCO, M-50) by spin coating solutions on silicon wafers. Each solution was directly spin coated onto cleaned quartz for NRET measurement.

In the fabrication of polymer nanotubes by the template wetting of polymer solutions, a clean AAO template was immersed in a PS-toluene solution (different concentrations result in different tube thicknesses) for 24 h. Subsequently, the template was picked up from the solution and dried at ambient conditions for 24 h and then in vacuum at room temperature for 24 h. Residual polymer layers on the AAO template were scraped off by a sharp blade. The samples were further annealed at 120 °C under vacuum for 2 h to ensure that there was no residual solvent.

The AAO templates with PS nanotubes were immersed in an aqueous sodium hydroxide solution (1.0 mol/L) for 24 h to remove the templates. After filtration and washing, the PS nanotubes were dried under vacuum at room temperature to remove the residual water. The polymer tube thicknesses were obtained from the SEM images and calculations.

C. Differential scanning calorimeter (DSC) measurements

The measurement was run on a Metter-Toledo DSC1 STAR system with a FRS5 sensor under a dry nitrogen atmosphere (N_2 flow of 50 mL/min). The instrument was calibrated with indium and zinc standards. Temperature programs were made as follows: All samples were first heated from 50 °C to 150 °C at 10 °C/min, held for 2 min at 150 °C, cooled from 150 °C to 50 °C at 10 °C/min (or 1 °C/min), and held for 2 min at 50 °C. The procedure was repeated thrice. The midpoint of the slope change of the heat capacity plot was taken as the glass transition temperature.

D. Fluorescence nonradiative energy transfer (NRET) measurements

Equal weights of PS-An and PS-Cz were dissolved in toluene at room temperature to obtain a homogeneous solution. The PS nanotube samples for NRET measurement were prepared as those for DSC measurement described above. The fluorescence spectrum was determined with a fluorometer (PTI, QM40) at an excitation wavelength of 294 nm, which was readily absorbed by Cz but not by An. All samples were measured at room temperature.

III. RESULTS

The strong dependence of the dynamics on the film thickness has encouraged many groups to focus their research on the thickness dependence of T_g of confined films [1–10,21,22,35–37]. While most confinement studies were dedicated to thin film geometries, only a few were conducted on thin films on a concave surface, such as in nanotubes [14]. The nanotube process is favored by low molecular weight PS infiltrated in AAO pores, while nanorods are mostly observed with large molecular weights [14]. According to previous reports [38], polymer nanotubes can be prepared by either melt wetting or solution wetting the templates. Here we used PS_{6k} (with a molecular weight of 6000 g/mol) in solutions (at different concentrations) to infiltrate the AAO templates of different pore sizes. After evaporating the solvent, nanotubes with different diameters (d) and tube thicknesses (δ) were prepared. Usually, Rayleigh instabilities can occur in polymer thin films confined in nanoporous alumina templates when heating to the melt state, and the characteristic time for the fastest growing mode decreases with increasing annealing temperature [39]. In our experiment, we did not anneal the nanotubes at very high

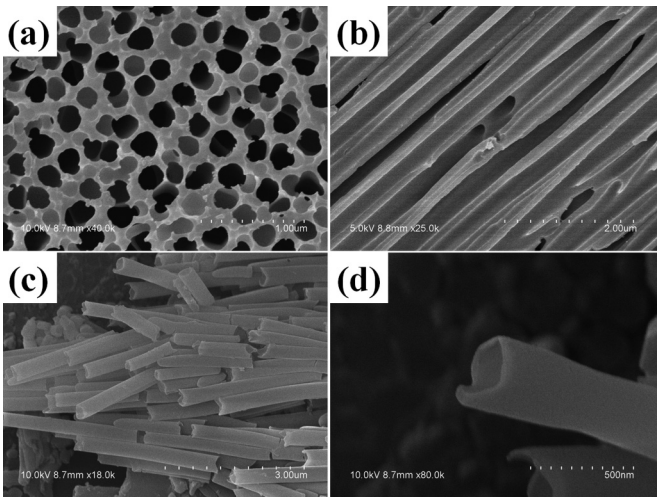

FIG. 1. SEM images for PS nanotubes in 250-nm AAO: (a) bottom view, (b) section view. After removing the AAO templates, PS nanotubes were clearly identified: (c) a bunch of PS nanotubes and (d) one typical detailed nanotube.

temperatures for a long time, so the nanotubes did not show obvious surface undulation. The scanning electron microscope (SEM) images of PS nanotubes are shown in Fig. 1, whereas the schematics for the structures of PS nanotubes confined in AAO nanopores are shown in Fig. 2. We can clearly see that the samples are nanotubes. Their T_gs were recorded by DSC, and the interchain proximity in the nanotubes was investigated by the NRET method.

Figure 2(a) illustrates the DSC heating curves for nanotubes infiltrated in AAO nanopores with different diameters. It is clear that the T_g for the PS nanotube increased compared with the bulk value, and the deviation becomes larger when the diameter gets smaller. For the PS nanotube with diameter $d = 55$ nm, the T_g was increased by 18 °C. Such a large increase in the T_g of the PS nanotube was totally unexpected, as the T_gs of PS thin films typically decrease with reduced film thickness [25]. All samples were scanned three times to confirm that the T_gs were reliably measured. Actually, the T_g of the second heating scan was already stable. When preparing the PS nanotubes in AAO with different diameters, the templates were immersed in the same solution. A decrease in the AAO pore diameter would induce a reduction in the thickness of the PS nanotube. It is difficult to prepare samples with the same tube thickness in AAO with different diameters. For samples with different diameters, the thicknesses of polymer nanotubes were different. We should distinguish whether the tube diameter or the tube thickness of PS contributed to the increased T_g. We immersed the AAO template ($d = 250$ nm) in PS solutions at different concentrations to obtain samples with different polymer tube thicknesses. The role of thickness confinement on the vitrification of thin polymer films on flat substrates has been of interest for many years [25]. However, Fig. 2(b) shows little difference in the T_g for nanotubes with different tube thicknesses in the range of 11–23 nm. Therefore, the T_g of the film on a concave substrate is mainly dependent on the curvature radius.

The DSC heating curves (at 10 °C/min) for PS nanotubes infiltrated in AAO templates were subjected to different cooling rates. In Fig. 2(a), the samples had been cooled at 10 °C/min before the subsequent heating scan, while in Fig. 2(b), the samples had first been cooled from the melt at 1 °C/min before the heating scan, and then subjected to the same heating scan (10 °C/min). The obvious enthalpy relaxation peaks near the T_g in the heating curves can be detected after slow cooling, but the cooling rates (10 °C/min or 1 °C/min) showed no differences for the T_g values.

In fact, the glass transition behaviors of the polymer nanotubes after removing the AAO templates were also studied

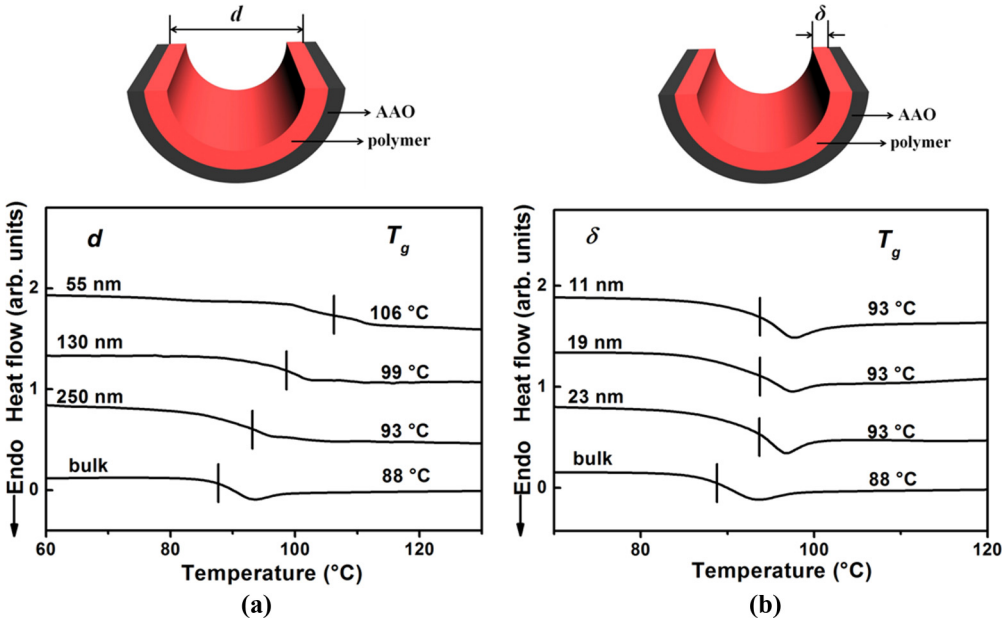

FIG. 2. (Color online) DSC heating curves (at 10 °C/min) for PS_{6k} nanotubes infiltrated in AAO templates. (a) T_g dependence on diameter (d) of the nanotubes; (b) T_g dependence on polymer tube thickness (δ) with the same pore diameter of 250 nm. The upper schematics show the structure of polymer nanotubes in AAO.

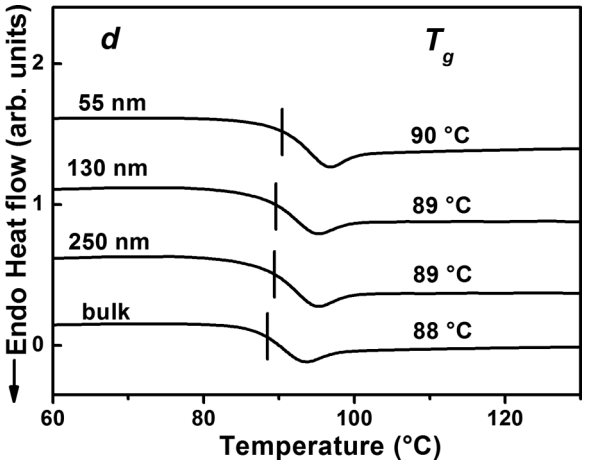

FIG. 3. DSC heating curves (at 10 °C/min) for PS_{6k} nanotubes after removing AAO templates.

with the DSC experiments, as shown in Fig. 3. It clearly indicates that the T_gs of PS nanotubes with different diameters almost all recover to the bulk value within the experimental error range. The samples were kept under a glassy state without any thermal treatment before the first heating scans. Therefore, compared to the results in Fig. 2, it can be concluded that the AAO hard wall is the main reason for the increase of T_g.

In order to further understand the glass transition dynamics changes induced by the confinement, we employed NRET methods to probe the interchain proximity, and thus the overall chain conformations. Two types of PS molecules were employed as probes: PS-Cz, which has a carbazolyl (Cz) moiety, and PS-An, which has an anthryl (An) moiety. Figure 4 shows the fluorescence spectra of PS-Cz, PS-An, and PS-blend (a 1:1 ratio blend by weight of the two molecules) nanotubes in 250-nm AAO, respectively. As expected, the intensity (I_A) of the fluorescence spectrum for PS-An was quite weak, whereas the intensity (I_C) for PS-Cz is quite strong. However, when the PS blend was excited, the spectrum showed a reduced intensity in the Cz band at 362 nm and an increased intensity

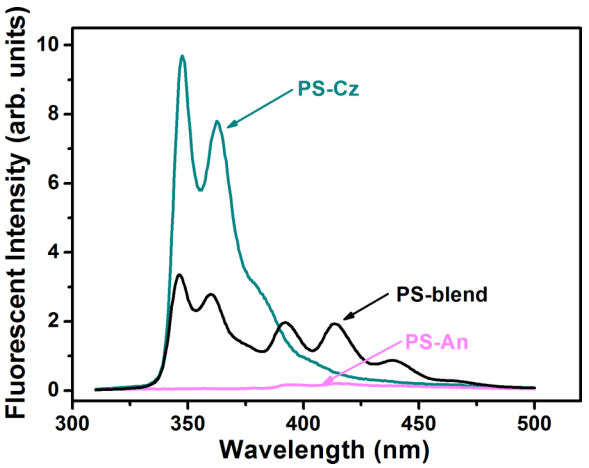

FIG. 4. (Color online) Fluorescence spectra from 6k PS-Cz, PS-An, and PS-blend nanotubes in 250-nm AAO templates. The excitation wavelength was 294 nm in each case.

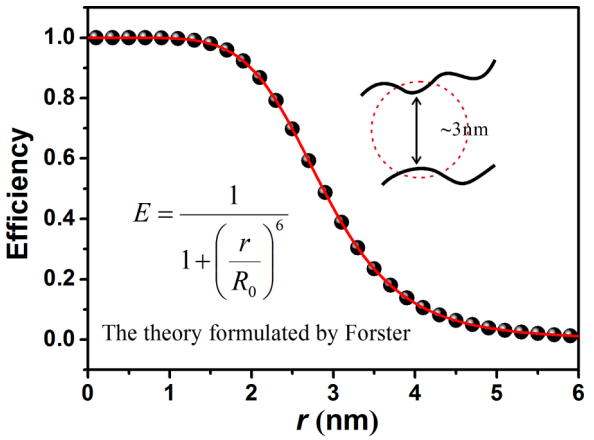

FIG. 5. (Color online) The relationship between the efficiency (E) of the nonradiative energy transfer and the distance (r) between donor and acceptor, which obeys the theory formulated by Forster [40].

in the An band at 414 nm. Actually, the excitation energy of the donor molecules (Cz) is transferred by a resonance dipole-dipole interaction mechanism over a distance to the acceptor molecules (An). Therefore, the fluorescent intensities of the acceptor will increase while that of the donor will decrease when the two moieties approach each other. As a result, the level of interchain proximity can be estimated by the ratio I_A/I_C (i.e., the fluorescence intensities of the acceptor and donor). The value of I_A/I_C is extremely sensitive to the separation distance between a donor and an acceptor and thus, is a measure of the interchain proximity. According to the theory formulated by Forster [40], the NRET method is very sensitive when the polymer interchain distance is around 3 nm. Figure 5 clearly shows the relationship between the NRET efficiency and the donor-accepter distance. Here, it is worth noting that the emission ratio can reveal the NRET efficiency but cannot be directly used to calculate the distance. So we cannot use the emission ratio to calculate the average r, and such large changes of the emission ratio I_A/I_C are reasonable. The details were also described in our recently published work [41].

As the intensity ratio I_A/I_C is directly related to the interchain proximity, it would be interesting to see the relationship between I_A/I_C and the polymer tube diameter, and thus to reveal the conformation changes induced by the confinement. As shown in Fig. 6(a), the ratio I_A/I_C increases for the PS nanotubes in the AAO template in comparison to the cast film, which indicates a decreased distance between the donor and acceptor. Besides, the ratio also increases as the tube diameter decreases, as shown in Fig. 6(b). This result well explains why the T_g increases for the PS nanotubes confined in AAO. The PS layer adsorbed on the hard wall has a reduced interchain proximity or interfacial free volume and thus results in the increase of T_g. In our previous work [31], we observed a double glass transition behavior for poly(methyl methacrylate) nanorods confined in AAO nanopores. A two-layer model showed that the polymer chains near the pore walls had a higher T_g due to the strong interfacial interaction and in the core center there was a reduced packing density which induced

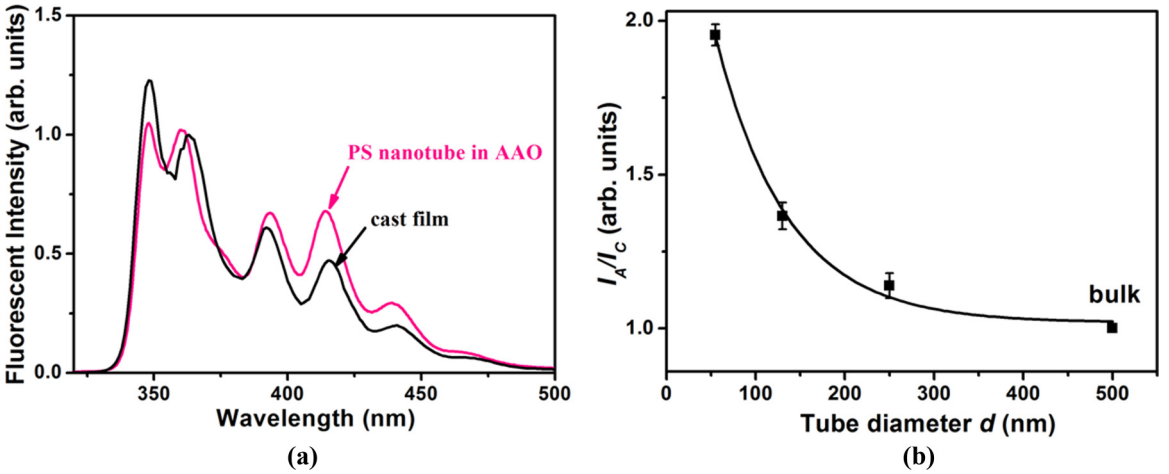

FIG. 6. (Color online) (a) Reflectance fluorescence spectra for solution-cast thick film (bulk polymer) and PS_{6k} nanotube in AAO templates. The intensity of the peak at 362 nm was normalized as 1. (b) The ratio I_A/I_C as a function of tube diameter.

a lower T_g. In our system, the PS nanotubes only show the glass transition behavior of the layer near the pore walls, so it is reasonable to expect an increased T_g.

In order to further understand the difference between supported polymer films and nanotubes, the T_g change (T_g-$T_{g(bulk)}$) and I_A/I_C as a function of the tube diameter before and after removing the AAO templates are shown in Fig. 7 as well as the T_g change and I_A/I_C as a function of the film thickness for supported PS_{6k} thin films. The T_g of the thin film was measured by differential alternating current (ac) chip

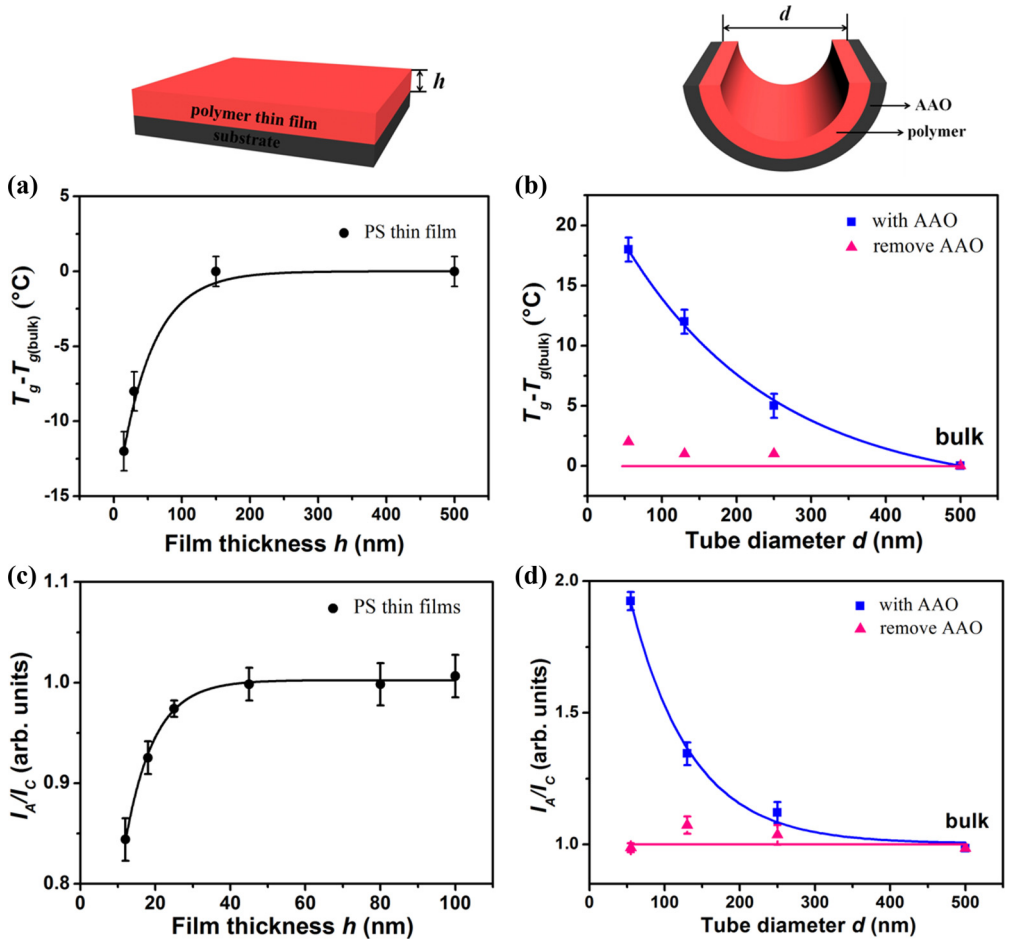

FIG. 7. (Color online) T_g-$T_{g(bulk)}$ dependence on (a) film thickness (supported PS_{6k} thin films) and (b) tube diameter (PS_{6k} nanotubes in and after removing AAO templates); I_A/I_C dependence on (c) film thickness (supported PS_{6k} thin films) and (d) tube diameter (PS_{6k} nanotubes in and after removing AAO templates).

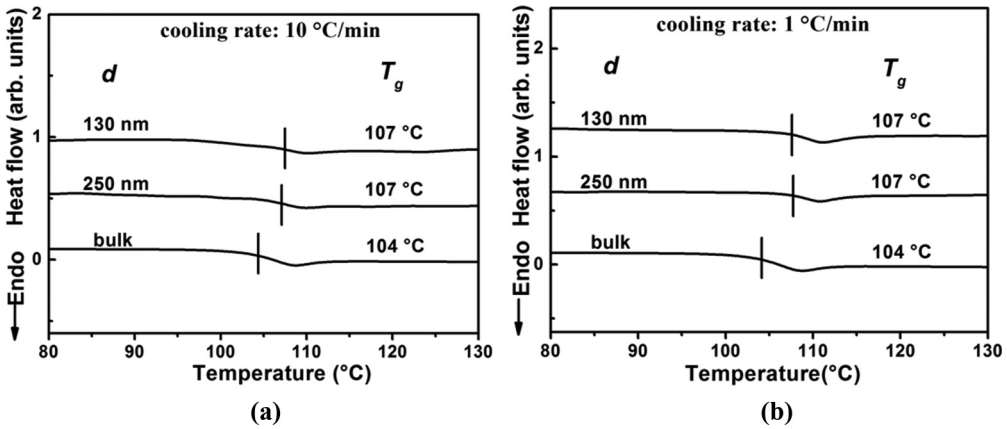

FIG. 8. PS_{60k} was infiltrated in AAO templates to form nanotubes, then heated to remove the heat history. DSC heating curves (at 10 °C/min) were recorded after the samples were cooled at (a) 10 °C/min or (b) 1 °C/min back to room temperature.

calorimetry, and the values were consistent with our current work [42].

It is clearly shown that the supported thin film and the concave nanotube have significantly different glass transition behaviors. For the supported polymer films, T_g-$T_{g(bulk)}$ and I_A/I_C decreased with decreasing film thickness, while both T_g-$T_{g(bulk)}$ and I_A/I_C of the PS nanotube increased as the tube diameter decreased, and converted back to the bulk values after removing the templates. The change in the T_g dynamics displayed a similar trend as that of the chain conformation for both of them. For supported thin film, the result is consistent with many previous reports [25]. However, our study reports such phenomena for confined polymer nanotubes. In particular, it is found that the different behaviors of PS_{6k} nanotubes before and after removing the templates are similar to the planar thin film system. Dalnoki-Veress *et al.* found that the T_g of free-standing film significantly increased when it was transferred back to the supported substrate [43]. These indicate the crucial importance of the interfacial effect imposed by the hard wall of the template.

The above studies were all based on low molecular weight PS (PS_{6k}). We also investigated the effect of molecular weight on properties of nanotubes. Figure 8 shows the T_g for PS_{60k} ($M_n = 60$ kg/mol) nanotubes infiltrated in AAO templates. Compared with the oligomer, the increased T_g for the PS_{60k} nanotube was not significant and only approximately 3 °C. The T_g did not further increase as the tube diameter decreased. It seems that the geometric confinement effect is not obvious for high molecular weight PS. The cooling rate (10 °C/min or 1 °C/min) also had no significant difference on the T_g. In our previous work [44], we detected the mobility and T_g for thiolated polystyrene (PS-SH) on gold nanoparticles (GNPs) and found that the molecular weight of PS-SH showed significant influence. As the results can be fitted with the core–two shell model, the inner shell was under strong constraints and the outer shell was less confined. For high molecular weight PS-SH, only a small part of the chains were confined in the inner shell; therefore the T_g showed little change from that of the bulk. We estimate that high molecular PS confined in AAO is similar to that on nanoparticles as described above. The wall effect is not as obvious for high molecular weight PS due to the longer chains.

IV. DISCUSSION

The T_gs of PS nanotubes in AAO were increased, and they all reverted back to the bulk value after removing the templates. In fact, Napolitano *et al.* proposed that the local free volume at buried polymer-substrate interfaces is strongly correlated with the changes in the T_g of ultrathin films [5,45], so the local free volume at the interface can influence the glass transition behavior of polymers under confinement. Our recent works on polymer thin films also confirmed that the interfacial free volume and mobility affect the glass transition behaviors [42,46]. Butt *et al.* reported that the free volume voids in the film between gold surfaces have a slightly smaller average size than in the bulk, resulting in a higher density at the polymer–solid substrate interface [47]. Wang *et al.* used Monte Carlo simulation to find that free chains confined in concave brush-coated nanocylinders are stretched in the axial direction and the end-to-end distance increases with decreasing pore radius [48]. Herein, on the basis of our experimental results, we deduced that the hard wall imposed a crucial effect to the adsorbed polymer layer and induced the variations in the T_g behaviors, while the effect was enhanced as the pore diameter decreased.

Boucher *et al.* reported that DSC delivers thermal and volumetric information, respectively, on the equilibrium to out-of-equilibrium transition marked by T_g. They observed T_g depression but invariant segmental dynamics for thin films. In our work, we observed an increased T_g for PS nanotubes confined in AAO templates by DSC. It reflects another geometric confinement. The tendency was different from the planar thin film, however reasonable. The NRET method detected the interchain proximity and overall chain conformation. The T_g results and chain conformation agreed well with each other. However, the existing results cannot be directly associated with the segmental dynamics since we did not take measurements such as dielectric spectroscopy. It is important to understand the difference of glass transition behaviors between the planar thin film and the nanotube. In contrast to the planar film where the properties are thickness dependent, the polymer concave film shows that the conformation and the T_g are mainly dependent on geometric curvature radius as discussed above, whereas in the narrow range of tube thickness of PS nanotubes we investigate here, the tube thickness has negligible effect.

However, this does not indicate that the tube thickness has no effect when the thickness further increases. For example, for the nanorod, where the template is fully filled with polymer, the glass transition behavior is completely different from that of nanotube. Huber *et al.* [49] reported the filling-fraction-dependent dielectric measurements on methanol confined in parallel-aligned channels in a mesoporous silica membrane, and found that T_g decreased upon filling from 3% to 43%, which was a wide range. It also indicated that the inner channel surface had a crucial effect on the T_g of methanol. Many reports showed that the geometric curvature had an important influence on the properties of confined samples, mostly in nanoparticle systems. Kraatz *et al.* [50] investigated the effect of the surface curvature on the secondary structure of peptides adsorbed on gold nanoparticles (GNPs). They found that the peptide remained helical on a flat gold surface but changed to another conformation on GNPs. As the surface curvature was reduced by increasing the size of the GNPs, the conformation gradually recovered to the native helical structure [50]. In our system, the T_g of PS_{6k} confined in AAO templates gradually increased as the inner surface curvature was increased by reducing the tube diameter. If the tube diameter is large enough, the T_g will behave as the bulk.

A hard wall also exerts significant influences over the structural properties of polymer glass [20]. For planar supported thin films, the tensile stress caused by spin coating would stretch the polymer chain networks parallel to the substrate and enlarge the interchain distance. So the NRET ratio decreased with respect to the bulk. Similar results about the chain stretch in planar polymer thin films were reported in our previous work [41]. The simulations also revealed that inside the range of the substrate potential there was a preferential orientation of the bonds parallel to the substrate surface [51].

However, for PS nanotubes in AAO template (curved substrate), the effect was different. Shin *et al.* [17] investigated the mobility of polymers confined within nanoscopic cylindrical pores and observed a chain contraction perpendicular to the nanopore axis as detected by the SANS method. After flowing into the pores the chains were not stretched in the direction of flow, but were compressed in a direction orthogonal to the flow owing to confinement. Recently, from the simulations, Tung *et al.* [52] also found that chain conformations parallel to the cylinder axis were elongated relative to the bulk conformation, whereas in perpendicular direction the chain conformations were compressed, leading to a decrease in the extent of entanglement and slower local dynamics. Perpendicular to the cylindrical axis, monomer motion was suppressed by the adjacent wall. So our observed results of the increased T_g for the polymer in nanopores were reasonable and agreed with their conclusions. Unlike Shin and Tung's systems, in our polymer nanotube, entanglement was absent and the pore diameter was much larger than the R_g of PS. Watanabe and Tanaka revealed that the slower dynamics near a wall was induced by wall-induced enhancement of glassy structural order [53]. In our work, interchain proximity was decreased due to the compressive constraints as revealed by the NRET method, and thus the mobility was decreased which induced an increased T_g.

The chain stretch or compression can alter the distances between donor and acceptor molecules, as reflected by the NRET method. In comparison with the bulk state, the interchain proximity for planar substrate was increased, while that for concave substrate was decreased. Different geometric curvatures induce different degrees of interchain proximity, which greatly influence the T_g dynamics.

V. CONCLUSIONS

Overall, we demonstrated that the NRET method was an important tool for investigating the interchain proximity of polymer in nanoconfined systems. The spectroscopic data demonstrated in this study perfectly matched the calorimetric results and provided a different implication to understanding geometric confinement on dynamics. Our study directly and clearly showed that the concave hard wall imposed a crucial interfacial effect to the adsorbed thin film, and induced different vitrification behaviors from both the bulk and planar thin films. For polymer nanotubes, the conformation and T_g were mainly dependent on geometric curvature radius.

ACKNOWLEDGMENTS

The authors appreciate the financial support of the National Basic Research Program of China (973 program, Grant No. 2012CB821503), the National Natural Science Foundation of China (Grants No. 21274060, No. 21174062, No. 21404055, and No. 51133002), the foundation research project of Jiangsu Province (Grant No. BK20131269), and the Program for Changjiang Scholars and Innovative Research Team in University.

[1] C. J. Ellison and J. M. Torkelson, Nat. Mater. **2**, 695 (2003).
[2] J. A. Forrest, K. Dalnoki-Veress, J. R. Stevens, and J. R. Dutcher, Phys. Rev. Lett. **77**, 2002 (1996).
[3] J. L. Keddie, R. A. L. Jones, and R. A. Cory, Faraday Discuss. **98**, 219 (1994).
[4] G. B. McKenna, Eur. Phys. J.: Spec. Top. **141**, 291 (2007).
[5] S. Napolitano and M. Wubbenhorst, Nat. Commun. **2**, 260 (2011).
[6] K. Paeng, S. F. Swallen, and M. D. Ediger, J. Am. Chem. Soc. **133**, 8444 (2011).
[7] Z. H. Yang, Y. Fujii, F. K. Lee, C. H. Lam, and O. K. C. Tsui, Science **328**, 1676 (2010).
[8] G. Reiter, M. Hamieh, P. Damman, S. Sclavons, S. Gabriele, T. Vilmin, and E. Raphael, Nat. Mater. **4**, 754 (2005).
[9] J. E. Pye and C. B. Roth, Phys. Rev. Lett. **107**, 235701 (2011).
[10] D. Qi, Z. Fakhraai, and J. A. Forrest, Phys. Rev. Lett. **101**, 096101 (2008).
[11] P. Rittigstein, R. D. Priestley, L. J. Broadbelt, and J. M. Torkelson, Nat. Mater. **6**, 278 (2007).
[12] C. Zhang, Y. L. Guo, and R. D. Priestley, Macromolecules **44**, 4001 (2011).
[13] D. Bae, G. Jeon, H. Jinnai, J. Huh, and J. K. Kim, Macromolecules **46**, 5301 (2013).

[14] L. Noirez, C. Stillings, J. F. Bardeau, M. Steinhart, S. Schlitt, J. H. Wendorff, and G. Pepy, Macromolecules **46**, 4932 (2013).
[15] J. Byun, Y. Kim, G. Jeon, and J. K. Kim, Macromolecules **44**, 8558 (2011).
[16] M. Krutyeva, A. Wischnewski, M. Monkenbusch, L. Willner, J. Maiz, C. Mijangos, A. Arbe, J. Colmenero, A. Radulescu, O. Holderer, M. Ohl, and D. Richter, Phys. Rev. Lett. **110**, 108303 (2013).
[17] K. Shin, S. Obukhov, J. T. Chen, J. Huh, Y. Hwang, S. Mok, P. Dobriyal, P. Thiyagarajan, and T. P. Russell, Nat. Mater. **6**, 961 (2007).
[18] K. F. Freed and C. Wu, J. Chem. Phys. **135**, 144902 (2011).
[19] D. Chen, W. Zhao, and T. P. Russell, ACS Nano **6**, 1479 (2012).
[20] J. Baschnagel and K. Binder, Macromolecules **28**, 6808 (1995).
[21] J. H. Jang and W. L. Mattice, Polymer **40**, 4685 (1999).
[22] H. Tsuruta, Y. Fujii, N. Kai, H. Kataoka, T. Ishizone, M. Doi, H. Morita, and K. Tanaka, Macromolecules **45**, 4643 (2012).
[23] H. Aoki, K. Mori, and S. Ito, Soft Matter **8**, 4390 (2012).
[24] V. M. Boucher, D. Cangialosi, H. J. Yin, A. Schonhals, A. Alegria, and J. Colmenero, Soft Matter **8**, 5119 (2012).
[25] F. Kremer, M. Tress, and E. U. Mapesa, J. Non-Cryst. Solids **407**, 277 (2015).
[26] J. Martin, M. Krutyeva, M. Monkenbusch, A. Arbe, J. Allgaier, A. Radulescu, P. Falus, J. Maiz, C. Mijangos, J. Colmenero, and D. Richter, Phys. Rev. Lett. **104**, 197801 (2010).
[27] M. D. Ediger and J. A. Forrest, Macromolecules **47**, 471 (2014).
[28] J. M. Torkelson and S. R. Gilbert, Macromolecules **20**, 1860 (1987).
[29] H. Morawetz, Science **240**, 172 (1988).
[30] H. Itagaki, Y. Nishimura, E. Sagisaka, and Y. Grohens, Langmuir **22**, 742 (2006).
[31] L. L. Li, D. S. Zhou, D. H. Huang, and G. Xue, Macromolecules **47**, 297 (2014).
[32] M. Hofmann, A. Herrmann, S. Ok, C. Franz, D. Kruk, K. Saalwaechter, M. Steinhart, and E. A. Roessler, Macromolecules **44**, 4017 (2011).
[33] S. Alexandris, G. Sakellariou, M. Steinhart, and G. Floudas, Macromolecules **47**, 3895 (2014).
[34] C. Y. Liu and H. Morawetz, Macromolecules **21**, 515 (1988).
[35] R. L. Jones, S. K. Kumar, D. L. Ho, R. M. Briber, and T. P. Russell, Nature **400**, 146 (1999).
[36] M. K. Mukhopadhyay, X. Jiao, L. B. Lurio, Z. Jiang, J. Stark, M. Sprung, S. Narayanan, A. R. Sandy, and S. K. Sinha, Phys. Rev. Lett. **101**, 115501 (2008).
[37] J. Kraus, P. Muller-Buschbaum, T. Kuhlmann, D. W. Schubert, and M. Stamm, Europhys. Lett. **49**, 210 (2000).
[38] M. Steinhart, J. H. Wendorff, A. Greiner, R. B. Wehrspohn, K. Nielsch, J. Schilling, J. Choi, and U. Gosele, Science **296**, 1997 (2002).
[39] J. T. Chen, M. F. Zhang, and T. P. Russell, Nano Lett. **7**, 183 (2007).
[40] T. Forster, Ann. Phys. **2**, 55 (1948).
[41] J. Xu, L. Ding, J. Chen, S. Gao, L. Li, D. Zhou, X. Li, and G. Xue, Macromolecules **47**, 6365 (2014).
[42] J. Chen, L. L. Li, D. S. Zhou, J. Xu, and G. Xue, Macromolecules **47**, 3497 (2014).
[43] O. Baumchen, J. D. McGraw, J. A. Forrest, and K. Dalnoki-Veress, Phys. Rev. Lett. **109**, 055701 (2012).
[44] L. L. Zhu, X. L. Wang, Q. Gu, W. Chen, P. C. Sun, and G. Xue, Macromolecules **46**, 2292 (2013).
[45] S. Napolitano, C. Rotella, and M. Wubbenhorst, ACS Macro Lett. **1**, 1189 (2012).
[46] J. Chen, J. Xu, X. L. Wang, D. S. Zhou, P. C. Sun, and G. Xue, Macromolecules **46**, 7006 (2013).
[47] H. J. Butt, H. Duran, W. Egger, F. Faupel, V. Harmandaris, S. Harms, K. Johnston, K. Kremer, F. Y. Lin, L. Lue, C. Ohrt, K. Raetzke, L. Ravelli, W. Steffen, and S. D. B. Vianna, Macromolecules **47**, 8459 (2014).
[48] R. Wang, S. A. Egorov, A. Milchev, and K. Binder, Macromolecules **45**, 2580 (2012).
[49] A. V. Kityk, P. Huber, R. Pelster, and K. Knorr, J. Phys. Chem. C **118**, 12548 (2014).
[50] H. S. Mandal and H. B. Kraatz, J. Am. Chem. Soc. **129**, 6356 (2007).
[51] C. Batistakis, A. V. Lyulin, and M. A. J. Michels, Macromolecules **45**, 7282 (2012).
[52] W.-S. Tung, R. J. Composto, R. A. Riggleman, and K. I. Winey, Macromolecules **48**, 2324 (2015).
[53] K. Watanabe, T. Kawasaki, and H. Tanaka, Nat. Mater. **10**, 512 (2011).